

Carderock Division
Naval Surface Warfare Center

Bethesda, Maryland 20884-5000

CDNSWC/TR-61-97-08 April 1997

Metals Department
Research and Development Report

**A Novel System for Miniature and Micro
Specimen Fatigue and Fracture Testing**

by
G.P. Mercier and
R.L. Tregoning

DTIC QUALITY INSPECTED 4



Approved for public release, April 1997. Distribution is
unlimited.

19970908 088

REPORT DOCUMENTATION PAGE

Form Approved
OMB No. 0704-0188

Public reporting burden for this collection of information is estimated to average 1 hour per response, including the time for reviewing instructions, searching existing data sources, gathering and maintaining the data needed, and completing and reviewing the collection of information. Send comments regarding this burden estimate or any other aspect of this collection of information, including suggestions for reducing this burden, to Washington Headquarters services, Directorate for Information Operations and Reports, 1215 Jefferson Davis Highway, Suite 1204, Arlington, VA 22202-4302, and to the Office of Management and Budget, Paperwork Reduction Project (0704-0188), Washington, DC 20503.

1. AGENCY USE ONLY (Leave blank)		2. REPORT DATE April 1997	3. REPORT TYPE AND DATES COVERED Final
4. TITLE AND SUBTITLE A Novel System for Miniature and Micro Specimen Fatigue and Fracture Testing		5. FUNDING NUMBERS PE-61152N 95-1-6140-151 96-1-6140-161 97-1-6140-171	
6. AUTHOR(S) G.P. Mercier, R.L. Tregoning		8. PERFORMING ORGANIZATION REPORT NUMBER CDNSWC/TR-61-97-02	
7. PERFORMING ORGANIZATION NAME(S) AND ADDRESS(ES) Naval Surface Warfare Center Carderock Division Bethesda, MD 20084-5000		10. SPONSORING/MONITORING AGENCY REPORT NUMBER	
9. SPONSORING/MONITORING AGENCY NAME(S) AND ADDRESS(ES) Office of Naval Research (ONR 332) Ballston Center Tower One 800 North Quincy Street Arlington, VA. 22217-5660		11. SUPPLEMENTARY NOTES	
12a. DISTRIBUTION/AVAILABILITY STATEMENT Approved for public release; distribution is unlimited.		12b. DISTRIBUTION CODE Distribution Code A	
13. ABSTRACT (Maximum 200 words) A microspecimen testing system has been developed to conduct real-time fatigue and fracture measurement on specimens less than 1mm thick. Principal components include an interferometric-based crack opening displacement (COD) gage, a piezoelectric actuator, a resistive load cell, and an integrally machined testing cell and loading fixtures. Software has been developed to rapidly analyze interference signals and provide close-loop cyclic control. The principal system limitation is that the maximum real-time cyclic testing frequency is only 1/4 Hz for the relatively large specimens tested. System measurement resolution based on the load, COD, and load-line displacement is adequate for B = 1mm SE(B) specimens, and illustrates the capability to test much smaller specimens. Initial system testing has indicated the following: the effects of planar rigid body motion have been simply discriminated from actual COD, compliance estimates based on these COD readings are accurate for a/W = 0.5, and system stability appears to be reasonable.			
14. SUBJECT TERMS Miniature Specimen, Interferometry, Micro Specimen Fatigue Crack Growth Rate, Fracture Testing, HSLA-100			15. NUMBER OF PAGES 19
17. SECURITY CLASSIFICATION OF REPORT UNCLASSIFIED			16. PRICE CODE
18. SECURITY CLASSIFICATION OF THIS PAGE UNCLASSIFIED	19. SECURITY CLASSIFICATION OF ABSTRACT UNCLASSIFIED	20. LIMITATION OF ABSTRACT SAR	

CONTENTS

CONTENTS	iii
FIGURES	iv
ABSTRACT	v
ADMINISTRATIVE INFORMATION	v
ACKNOWLEDGEMENTS	v
INTRODUCTION	1
MICROTESTING SYSTEM	2
The Load Train and Specimen Design	2
Crack Opening Measurement	3
COD Gage: Overview	3
COD Gage: Electronic Hardware	4
Data Acquisition System	5
Hardware	5
Software	6
SYSTEM CALIBRATION	7
COD Gage and Rigid Body Motion	7
System Testing: Compliance Calibration & Stability	8
ONGOING AND FUTURE RESEARCH	10
CONCLUSIONS	10
REFERENCES	19

FIGURES

Number	Title	Page
<i>Figure 1</i>	<i>Schematic of System Components</i>	<i>12</i>
<i>Figure 2</i>	<i>Basic Test Set-up</i>	<i>12</i>
<i>Figure 3</i>	<i>Test Machine and Specimen</i>	<i>13</i>
<i>Figure 4</i>	<i>Geometric Construction Describing Fringe Patterns</i>	<i>13</i>
<i>Figure 5</i>	<i>Micro-hardness Indentations</i>	<i>14</i>
<i>Figure 6</i>	<i>Data Acquisition System Logic</i>	<i>15</i>
<i>Figure 7</i>	<i>Rigid Body Motion in the X Direction</i>	<i>16</i>
<i>Figure 8</i>	<i>Combined Rigid Body Motion</i>	<i>16</i>
<i>Figure 9</i>	<i>Frictional Effects on Fatigue Cycling</i>	<i>17</i>
<i>Figure 10</i>	<i>Compliance Estimates During Quasistatic Loading</i>	<i>17</i>
<i>Figure 11</i>	<i>System Stability</i>	<i>18</i>

ABSTRACT

A microspecimen testing system has been developed to conduct real-time fatigue and fracture measurement on specimens less than 1mm thick. Principal components include an interferometric-based crack opening displacement (COD) gage, a piezoelectric actuator, a resistive load cell, and an integrally machined testing cell and loading fixtures. Software has been developed to rapidly analyze interference signals and provide close-loop cyclic control. The principal system limitation is that the maximum real-time cyclic testing frequency is only $\frac{1}{4}$ Hz for the relatively large specimens tested. System measurement resolution based on the load, COD, and load-line displacement is adequate for $B = 1\text{mm SE(B)}$ specimens, and illustrates the capability to test much smaller specimens. Initial system testing has indicated the following: the effects of planar rigid body motion have been simply discriminated from actual COD, compliance estimates based on these COD readings are accurate for $a/W = 0.5$, and system stability appears to be reasonable.

ADMINISTRATIVE INFORMATION

This work was performed by the Fatigue and Fracture Branch of the Naval Surface Warfare Center as part of the "Mechanical Properties of Micro-Material" project sponsored by the Office of Naval Research ILIR program, PE 61152N, Task Area R0004, using work unit plans 95-1-6140-151, 96-1-6140-161 and 97-1-6140-171. The ILIR program manager was Dr. Bruce Douglas, Director of Research (NSWCCD), who was assisted by Dr. John Barkyoub, Code 60 ILIR Coordinator (NSWCCD 60). The work described herein was supervised by Mr. Thomas Montemarano, Head, Fatigue and Fracture Branch, NSWCCD 614.

ACKNOWLEDGEMENTS

The authors would like to thank Mr. A. Brandemarte of NSWCCD and Mr. D. Lavan of John's Hopkins University for their help on this project. Cliff Bennet of John's Hopkins University Applied Physics Laboratory was very helpful in the initial specimen and testing machine design. The discussions held with Professor William Sharpe of John's Hopkins University were also very fruitful.

INTRODUCTION

Various industries are exhibiting a heightened interest in evaluating mechanical properties using miniature test specimens. The nuclear industry is faced with limited surveillance capsule material for measuring radiation embrittlement effects over time. This shortfall is driving the development of a new sub-sized Charpy testing methodologies [1, 2]. The US Navy would also benefit from enhanced techniques to aid in failure analysis and material characterization. However, the burgeoning fields of miniature, micro (i.e., MEMS), and nano-electromechanical system design, manufacturing, and testing have the most immediate need for small-scale mechanical property evaluation.

These systems are based on silicon wafer manufacturing techniques developed originally for computer chip and electronic component production. While numerous prototype devices have been developed, there appears to be a general lack of knowledge about material behavior as the size-scale of the material decreases both absolutely and with respect to its microstructure. This knowledge is required for optimizing system design using fundamental material properties with machine design principles. However, experimental techniques must be developed and standardized for conducting mechanical testing on miniaturized, micro, and nano-scale materials.

Several researchers are currently developing techniques for measuring tensile properties [3, 4] which may also be suitable for evaluating un-cracked cyclic fatigue properties (e.g., S-N, e-N). There has been relatively little effort in developing similar techniques for measuring fatigue and fracture properties in the presence of a crack. Included herein is a synopsis of the development of a microspecimen testing system for evaluating cracked specimen behavior. The characteristics, calibration, and performance of this system are described under predominantly fatigue loading which provides the more stringent testing conditions. Initially, relatively large, 20 mm^3 , specimens were evaluated for ease of handling, but the system is tailored for testing much smaller specimens. Ongoing and future research are also discussed.

MICROTESTING SYSTEM

The micro-testing system is designed to operate in closed loop control using feedback from standard fracture parameters such as the stress intensity factor range (ΔK), the crack length change (Δa), the crack growth rate (da/dN), or the load range (ΔP). The micro-testing system consists of three primary subsystems (Figure 1): the load train and test cell, the crack opening displacement (COD) gage, and the data acquisition system. Each of these subsystems is described subsequently.

The Load Train and Specimen Design

The major components of the load train are the piezoelectric actuator, translation slide, resistive load cell, piston, specimen and test cell (Figure 2). Specimen loading occurs via the piezoelectric actuator which can produce up to 3500 N of compressive force and 500 N of tensile force. The actuator response is limited only by the speed of sound in the quartz element and the resolution is largely dependent on the amplifier characteristics which makes it ideal for high frequency, high resolution testing. One minor drawback is that the total displacement range is restricted to 180 μm . While this range is adequate for testing most miniature specimens, larger specimens (10 - 20 mm^3) made of more ductile materials require more displacement in order to measure a complete J-R curve. Precise actuator alignment with the test cell is necessary due to the low shear strength of the piezoelectric's ceramic element. This was accomplished by mounting the actuator to a three position translation stage which has a resolution of 2 μm and is rated to withstand 900 N in the loading direction.

A resistive load cell mates the actuator to a specially electrodischarged machined (EDM) piston (Figure 3). The piston threads onto the load cell and is positioned within a square entry hole in the test cell. The piston shank is square to facilitate manufacture, and the contact end or tup is rounded, as per ASTM standards, to accurately load the test specimen along its centerline. The load cell capacity is 100 N which is adequate for the current specimens tested, however, smaller cells with ranges down to 0.5 N and below will be used for testing specimens down to 100 μm in thickness.

The current specimen material is a high strength low alloy (HSLA-100) naval structural steel which has been austenized and tempered to produce a fine equiaxed microstructure with an ASTM grain size number of 10. The small equiaxed grains create a homogeneous, isotropic, model material at the small length scales tested and facilitates fracture analysis using conventional continuum mechanics or emerging micromechanical techniques [5, 6]. The HSLA-100 SE(B) microspecimen is 1 mm thick x 2 mm wide x 9 mm long. The notch was machined with a 0.25 mm EDM wire and the top surface was polished to a six micron finish. Figure 3 shows the specimen inserted in the test machine with the piston just touching the specimen's back surface. The specimen rests on two hardened, tool steel rollers which are seated in grooves machined in the test cell. Fixing the roller position aids in alignment and also maintains the proper initial span.

Crack Opening Measurement

A major difficulty in conducting fracture tests on miniature specimens is crack opening displacement measurement. This measurement is difficult because the gage length must be small and fine resolution is imperative. Conventional contacting devices (e.g., clip gages, capacitance sensors, etc.) are impractical. They are nearly impossible to physically attach and their potential effect on the measured specimen stiffness and load is a concern. Therefore, a laser based, non-contacting COD gage was chosen. The gage length can be less than 100 μm [7] and has a reported displacement resolution of 0.02 μm [8]. Originally developed for optical strain measurement [9], improvements in the technique and equipment have increased measurement resolution and made the technique viable for automated testing [7, 10].

COD Gage: Overview

The COD gage is based on Young's two-slit interference principle [11]. Consider two adjacent slits which are separated by a distance, d (Figure 4). Coherent light diffracted through each slit travels a different distance before arriving at point A on the image plane. The path length difference, $d\sin\theta$, produces either constructive or destructive interference between the two diffracted beams at point A. Changes in the slit distance, Δd , are then defined simply by

$$\Delta d = \frac{\Delta m \lambda}{\sin \theta} , \quad [1]$$

where m is the fringe order, λ is the wavelength of the coherent light source and θ is the angle of incidence between the incoming laser beam and the image plane at point A [12].

The COD gage is based on the same principle in reflection. Coherent light impinges on two 30 μm square-based pyramidal indentations that have been pressed in the specimen's surface with a Vickers micro-hardness tester (Figure 5). The indents are placed on either side of the specimen's machined notch at a spacing of approximately 500 μm . Interference patterns form upon reflection from the indent face and interference pattern motion is governed by equation 1, with $\text{COD} = \Delta d$. The coherent light source is a 30 mW He-Ne laser with a 632.8 nm wavelength, and the angle of reflection from the pyramidal indentation face is approximately 42°. Therefore, the 'calibration factor' ($\lambda/\sin\theta$) in equation 1 is 0.95 μm , and is equivalent to the interference pattern wavelength.

It is important to note that it is the relative motion of the interference patterns that is being measured, not the intensity. The interference signal's intensity varies naturally due to modulation from each indent's diffraction pattern. 'Speckle spots' also form on the fringe patterns during testing as slip increases the indentation surface roughness. The end result is that the intensity level of the extreme points fluctuates during the test and can lead to unreliable results. One disadvantage, however, in recording fringe motion is that each fringe minimum must be uniquely identified at each displacement increment. This restriction effectively limits the fringe shift to less than one wavelength per increment, and places an upper bound on the actuator step size. For the specimens tested here, a minimum of 200, 0.5 μm actuator steps were required to complete one loading cycle between 7.5 and 75 N ($\Delta K = 16.5 \text{ MPa}\sqrt{m}$).

COD Gage: Electronic Hardware

Two linear diode arrays (LDAs) were used to record the interference signals. These arrays consist of 512 silicon diode elements which store photoelectric charge and periodically output a proportional current. Each of the 512 diode elements is 25 μm wide by 2.5 mm long and is mounted on a single 16 pin chip. The LDA chip is mounted on a satellite board which is electronically controlled by a remote mother

board. In the current system, the LDAs were mounted perpendicularly to the light reflected from the specimen (Figure 2) and black electrical tape was placed around the diode border to reduce additional signal noise from stray reflections. Fourteen fringes orders were incident on the 512 element LDA which implies a maximum displacement resolution of 26 nm ($0.95\mu\text{m} \times 14/512$) between each element. This resolution is three orders of magnitude greater than is necessary for the specimen tested and would be sufficient for SE(B) specimens with a 1 μm thickness.

The effective data acquisition (DAQ) rate is dependent on the LDA signal acquisition process. The LDA process is triggered and regulated by a 200 kHz, software-controlled, transistor to transistor logic (TTL) clock signal generated by the DAQ board. This signal governs both the scan rate of individual diode elements and the integration time for storing photoelectric charge between scanning passes. The fixed scanning rate of 200 kHz requires 2.56 ms to record the entire LDA (512/200 kHz) output. The integration time is the number of TTL clock cycles between scanning passes and is manually set by 12 binary switches. The minimal setting of 516 was used to fix the integration time at 2.58 ms. Therefore, the total LDA signal acquisition rate is 194.5 Hz for each displacement increment and represents the maximum possible cyclic testing frequency. Other system limitations greatly reduce the achievable rate for real-time testing.

Data Acquisition System

Hardware

The data acquisition system platform is a 486-50 DX2 computer with 8 MB of RAM. The (DAQ) board has 12 bit resolution, dual counter/timer chips, supports both analog-to-digital (ADC) and digital-to-analog (DAQ) conversion, and has a maximum sequential sampling rate of 1.25 MS/s. Four analog channels are monitored in this test: the right and left interference signals, the load, and a trigger signal. Therefore, the actual DAQ signal input rate is 312.5 KS/s. The trigger signal is generated by the LDA mother board prior to every scanning pass and is used to synchronize data acquisition. The gain for each input channel is independent and has been selected to maximize the full 12 bit resolution of the board for each channel. One counter/timer is used as the clock for LDA signal acquisition, and DAQ output consists

of the TTL clock signal for LDA acquisition and the closed-loop feedback signal which governs the piezoelectric actuator motion.

Software

The fatigue loading software is designed to operate as six parallel processes (Figure 6). Process 1 records the analog load and fringe patterns signals sent to the DAQ board and performs an exponentially weighted sliding average to smooth the interference data. This process then stores the data into separate global arrays for access by the remaining processes. Process 2 locates the middle ten fringe pattern minima where the signal to noise ratio is the greatest. The minima are found by first dividing the LDA into 14 equivalent sections at predetermined element locations, and then searching for local minima within each section. Process 3 tracks the relative motion of each local minima by comparing their current with their previous locations and storing both the direction and magnitude of this difference. The shift arrays from each LDA sensor are then algebraically averaged to calculate the mean fringe order shift and simultaneously eliminate the rigid body motion contributions. The next process scales both the load voltage and mean fringe order shift into engineering load and COD values. This process also tracks the cycle number, N , and provides the actuator control signal for the next displacement increment. These first four loops process data during each actuator displacement increment.

The crack length is computed in process 5 after each cycle has been completed. The compliance for the cycle is first determined by a least squares linear fit to the loading portion of the cycle. Crack length is then calculated using standard ASTM equations [13]. This process is repeated for twenty-five cycles and an average crack length for this increment is determined. Using this average crack length, fracture parameters (i.e. J , K , $CTOD$) are then calculated in the sixth process using standard ASTM equations [13]. A new control load is then calculated and updated in process 4.

Unlike many conventional, sequential programs, these parallel processes all run simultaneously. The advantages of this structure is that new data can be recorded while previous data is analyzed. Further, the run time for a conventional program is dependent on the cumulative time of all of the loops and subroutines, while run-time for a parallel program is governed solely by the slowest process. Individual processes are also naturally isolated so that bottlenecks can be identified and relieved to streamline the

process. Some drawbacks of this parallel structure are that interactive decision-making occurs with data obtained during previous loading increments and therefore doesn't reflect the instantaneous loading state. Also, most software and hardware has not been optimized for parallel computing.

These characteristics impact this fatigue system (Figure 6) in a straightforward manner. If the current loading increment is i , control decisions are made during process 4 with data obtained during the $(i - 4)$ loading increment. While some load overshoot invariably occurs, the amount is inconsequential due to the small actuator step size requirement for COD measurement. Also, the current platform has only a single, sequential processor so that the overall program speed is not enhanced by its parallel structure. The relatively slow process times (Figure 6) reflect this limitation. The fringe shift calculation is the slowest procedure in this algorithm and requires 15 ms to complete. The average wait time for the LDA trigger which starts process 1 is 3.39 ms (half the time required for LDA scanning plus DAQ rate) so that the average DAQ time is approximately 18.4 ms per displacement increment. Recall that 200 displacement increments are required per loading cycle with the current test specimen, which limits the actual fatigue cycling rate to approximately $\frac{1}{4}$ Hz.

SYSTEM CALIBRATION

COD Gage and Rigid Body Motion

A coordinate system for the discussion of planar rigid body motion (RBM) of the specimen is defined in Figure 3. Out-of-plane motion is also possible during specimen expansion and contraction and crack tip plastic zone formation. However, the deformation level at the indentation sites is low [14,15] which implies that contributions from out-of-plane motion is inconsequential. Specimen planar RBM originates from elasticity in the fixtures and vibration or movement within the loading system. In order to eliminate rigid body motion effects, two LDAs are placed on either side of the specimen (Figure 2). Opposite signs are assigned to the fringe motion direction at each LDA and the measured displacement from the two sensors is algebraically averaged. Since RBM causes the fringes to move across the detectors in the same direction, its effect is canceled.

RBM in the X direction is the most nefarious because it is coincident with the COD axis. The effectiveness of the RBM elimination technique was demonstrated along this axis in the following manner. The specimen was placed on a linear translation stage and the laser was focused on the far right extreme of the indents. This extreme point was chosen where the signal to noise was low and the fringe pattern was only marginally discernible. The specimen was then translated along the X axis and fringe pattern displacement was recorded up to the far left extreme of the indents. No further signal processing was done. The slope of each individual interference fringe displacement measurement (Figure 7) exhibits an excellent one to one correlation with the actual specimen translation and almost complete RBM cancellation after averaging the two LDA measurements (Figure 8). The root mean squared (rms) average deviation of the measured displacement during this test was $5.1\text{ }\mu\text{m}$, which is only 0.17% of the 3.0 mm total translation stage travel.

A similar test was conducted to examine the effect of planar rigid body motion along the Y axis. As before, the laser light was focused at one extreme position on the indents. The specimen was then moved to the opposite extreme and back to the initial position. The results indicate (Figure 8) that when the laser light completely covered the microhardness indents, the averaged RBM was small. However, the scatter created by poor fringe signal quality at the extreme positions generated noise that overwhelmed the usable signal and must be avoided when testing. During the 2.4 mm section when the laser completely covered the indents, the averaged measured rms average deviation is $1.9\text{ }\mu\text{m}$ which is only 0.08% of the total specimen travel.

System Testing: Compliance Calibration & Stability

The microtest system fidelity was also evaluated by comparing the normalized crack length measured from compliance with the known normalized crack length (a/W). Initially, large inconsistencies between the measured and actual compliance were evident due to hysteresis. Fatigue cycling exacerbated the hysteresis loop and also increased differences between loading and unloading compliances (Figure 9). Only the lower portion of unloading within each cycle provided consistent, realistic crack length estimates. The hysteresis was also characterized by almost no increase in COD during initial loading until after a threshold load, P_{th} , was exceeded. Closer examination revealed that friction between the piston and test

cell was the primary reason for the hysteresis. The tolerance between the piston and test cell was increased and a molybdenum disulfide film was applied to the piston surface. This substantially reduced friction and the cyclic response (Figure 9) appears better conditioned. Some slight hysteresis is still evident near the load reversal points, but compliance estimates using solely the loading or unloading regions now differ by less than 5%.

The crack length measurement accuracy was then evaluated by quasistatically loading a specimen to 75% of its limit load, unloading completely, calculating compliance using every data point in the cycle, and then determining a/W from standard equations [13]. The calculated a/W differed by less than 5% from the machined a/W of 0.500 (Figure 10). However, if the individual loading or unloading portions of the curve were used for the calculation, the error was less than 1% for the loading portion and 5.6% for the unloading section. While the absolute difference in these two crack length estimates is only 0.05 mm, it is obvious that the loading portion of the cycle provides better estimates and that hysteresis near the load reversal point still contributes to some inaccuracy. All subsequent measurements use only the loading portion of the curve for crack length determination. While the accuracy of system at different crack lengths still needs to be rigorously proven these initial results are promising.

A displacement controlled test was also conducted to evaluate the stability of the test system (Figure 11). A SE(B) specimen was fatigued for 7000 cycles (8 hours) below the expected threshold ΔK to ensure a constant crack length. The specimen load remained constant during this test which implies that no measurable crack growth occurred. Over this test duration, some slight compliance variation was evident although the corresponding crack length variation was only 40 μm ($\Delta a/W = 0.02$), or 4% of the mean crack length. It is important to note that the output was relatively stable over this extended period and no significant system drift was evident. This result is a good indication of the durability of the interference signals, the stability of the measurement and amplification electronics, and the consistency of the analysis and control software. It also indicates that the physical characteristics (e.g., tolerances, stiffness, friction, etc.) of the testing system remain consistent and appear to be relatively unaffected by thermal or other long-term effects. These features bode well for long-term testing with this system.

ONGOING AND FUTURE RESEARCH

Based on the current system performance and limitations, several changes are currently being implemented. A new test cell and loading fixture design is being developed to decrease friction, increase loading sensitivity, and improve actuator alignment. The threaded connections between load cell and piston have been replaced by a simple compressive and/or magnetic interface junction which greatly reduces piezoelectric shear strain and makes precise actuator alignment less critical. A displacement amplification lever is being tested to amplify the piezoelectric range to conduct J-R curve testing of these large, 1 mm thick SE(B) specimens. The next generation piston will be supported by an air cushion to eliminate friction. Also, fixtures suitable for testing compact specimens have been designed. Software refinement is also ongoing to allow closed-loop J-R curve testing and increase the test frequency by further optimizing and evaluating each current bottleneck. Multiple processor platforms are also being explored.

More extensive testing of the current system is also being conducted. Several SE(B) specimens are being fatigue cycled at moderate ΔK levels, periodically beachmarked, grown to different final crack lengths, and then broken. The calculated crack lengths will then be compared to the measured crack lengths at each beachmark. If necessary, existing compliance expressions will be modified to correct for the difference between the crack mouth edge and the COD gage indentation locations. Once these changes have been implemented, and the integrity of the test system has been fully verified for large, 1 mm thick specimens, smaller (0.25 mm thick) MEMS-produced nickel specimens will be evaluated and compared to bulk material properties.

CONCLUSIONS

A microspecimen testing system has been developed for real-time fatigue and fracture property evaluation. The system consists of a resistive load cell, a test cell and loading fixtures produced from precision electrodischarge machining, an interferometric-based crack opening displacement gage, and a piezoelectric actuator. Analysis and control software has also been developed utilizing parallel architecture. The testing system has the following unique characteristics:

- The cyclic testing frequency for the 1 mm thick specimens tested is $\frac{1}{4}$ Hz. in “real-time” mode. While the raw signal acquisition rate is governed by the 195 Hz sampling rate of the LDAs, the data acquisition and analysis software limits the system’s bandwidth to 50 Hz. The incremental displacement limitation of the COD gage reduces this bandwidth down to the stated value for a complete loading cycle.
- The interference-based COD gage resolution is limited only by the ability to resolve fractional wavelength motion. In these tests, the linear diode array element spacing imposes a minimum threshold of 28 nm. The COD gage has been configured to discriminate planar rigid body motion from COD and has proven to be capable of this over a 3 mm range. This range appears to be limited only by the laser beam diameter.
- The measurement technique also appears to be suitable for testing smaller, less than 0.1 mm thick, SE(B) specimens. Each order of magnitude decrease in specimen thickness dictates a similar decrease in load-line and COD displacement range, and two orders of magnitude decrease in the loading range. These requirements are well above the inherent resolution of the COD gage. Further, the piezoelectric actuator and load cell exhibited linearity and resolution of less than 0.2% of full scale. Decreasing the range to 10 μ m for the piezoelectric and 1 N for the load cell should not affect this performance.
- The measurement stability of the system over a 7000 cycle or 8 hour time-frame was reasonable. The variation in crack length was less than 4% and remained consistent; there was no apparent drift as testing proceeded. This infers that the interference signal is durable, the measurement and amplification electronics are stable, and the software analysis is consistent. It also indicates that thermal or other long term effects do not physically impede the operation.
- The role of friction in small-scale testing cannot be underestimated. Initially, friction within the testing cell contributed to roughly 50% of the measured load and caused hysteresis in the load vs. COD response. Minimizing friction decreased the differences between the loading and unloading compliance measurements. Further, accurate, repeatable compliance estimations at $a/W = 0.5$ when then possible using only the loading portion of the cyclic response.

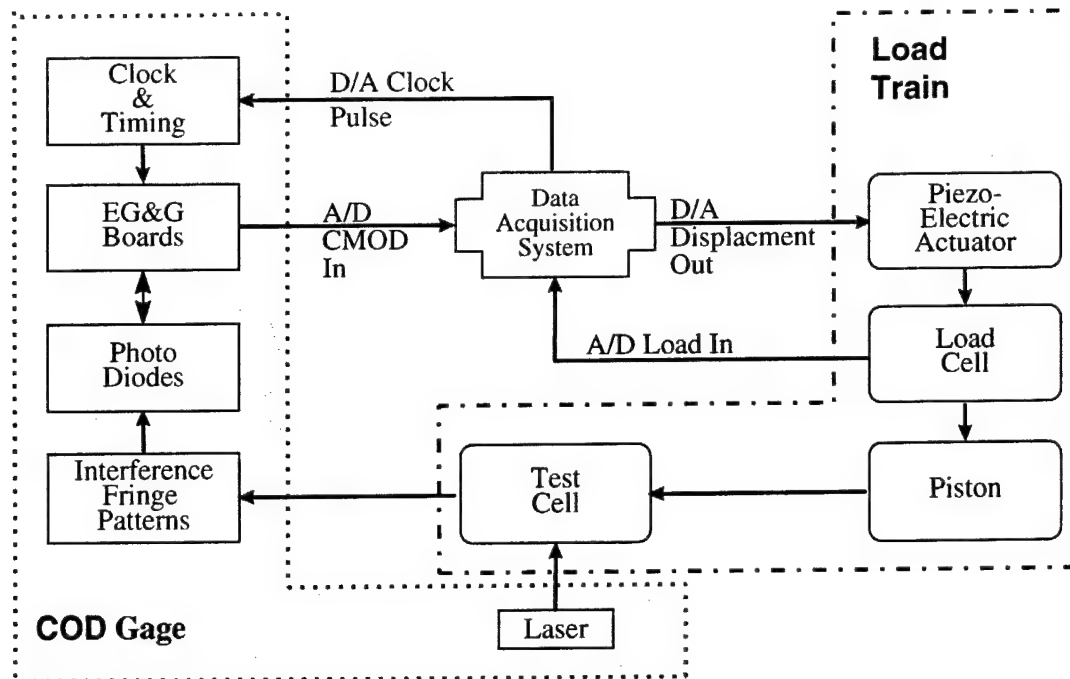


Figure 1
Schematic of System Components

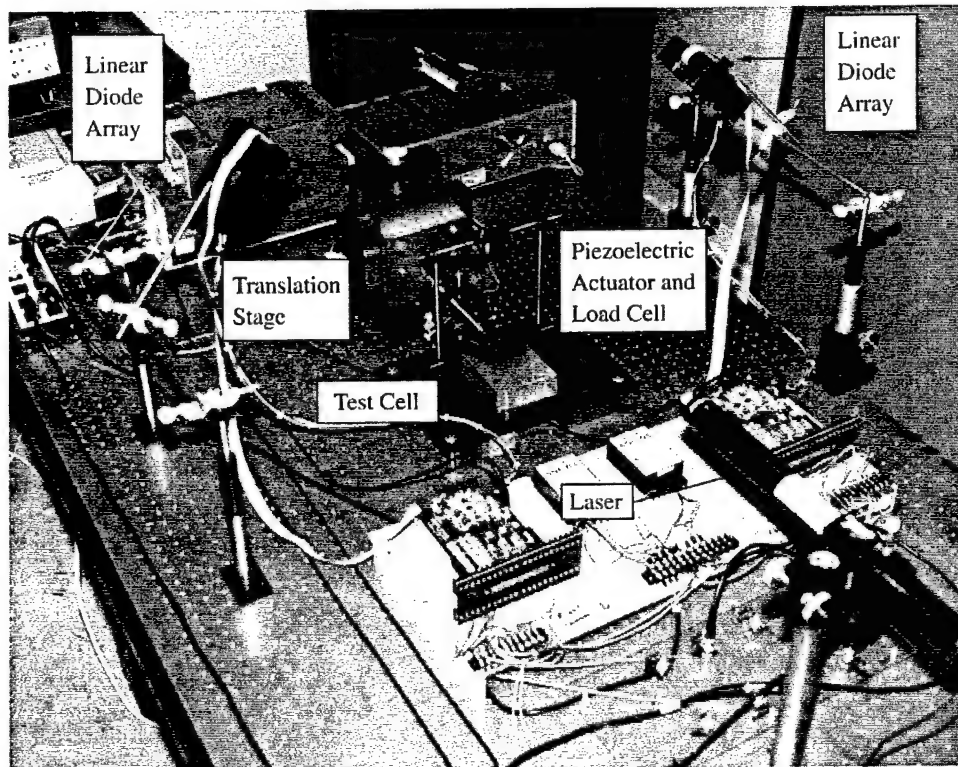


Figure 2
Basic Test Set-up

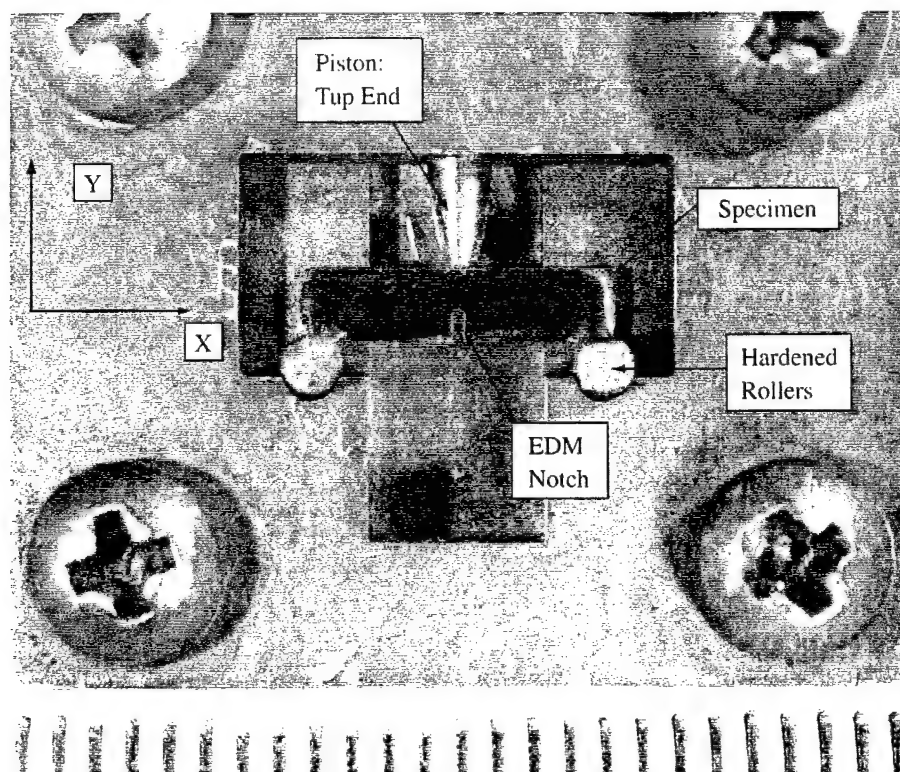


Figure 3
Test Machine and Specimen

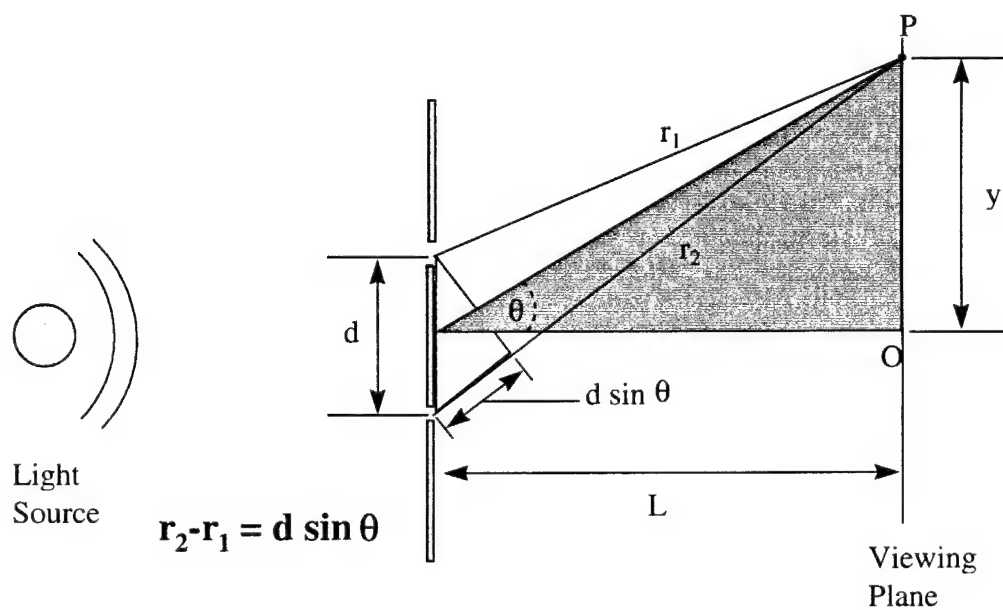


Figure 4
Geometric Construction Describing Fringe Patterns

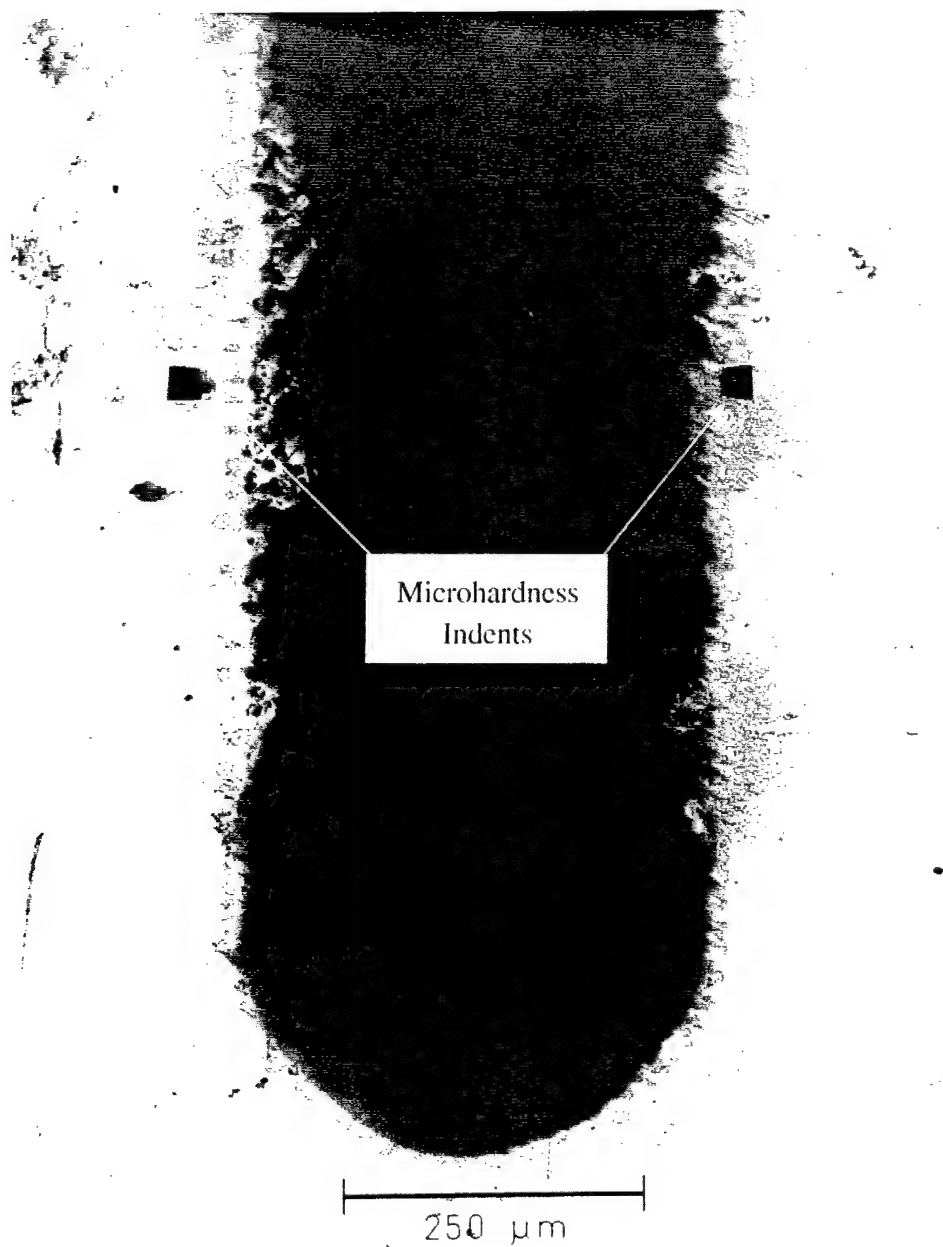


Figure 5
Micro-hardness Indentations

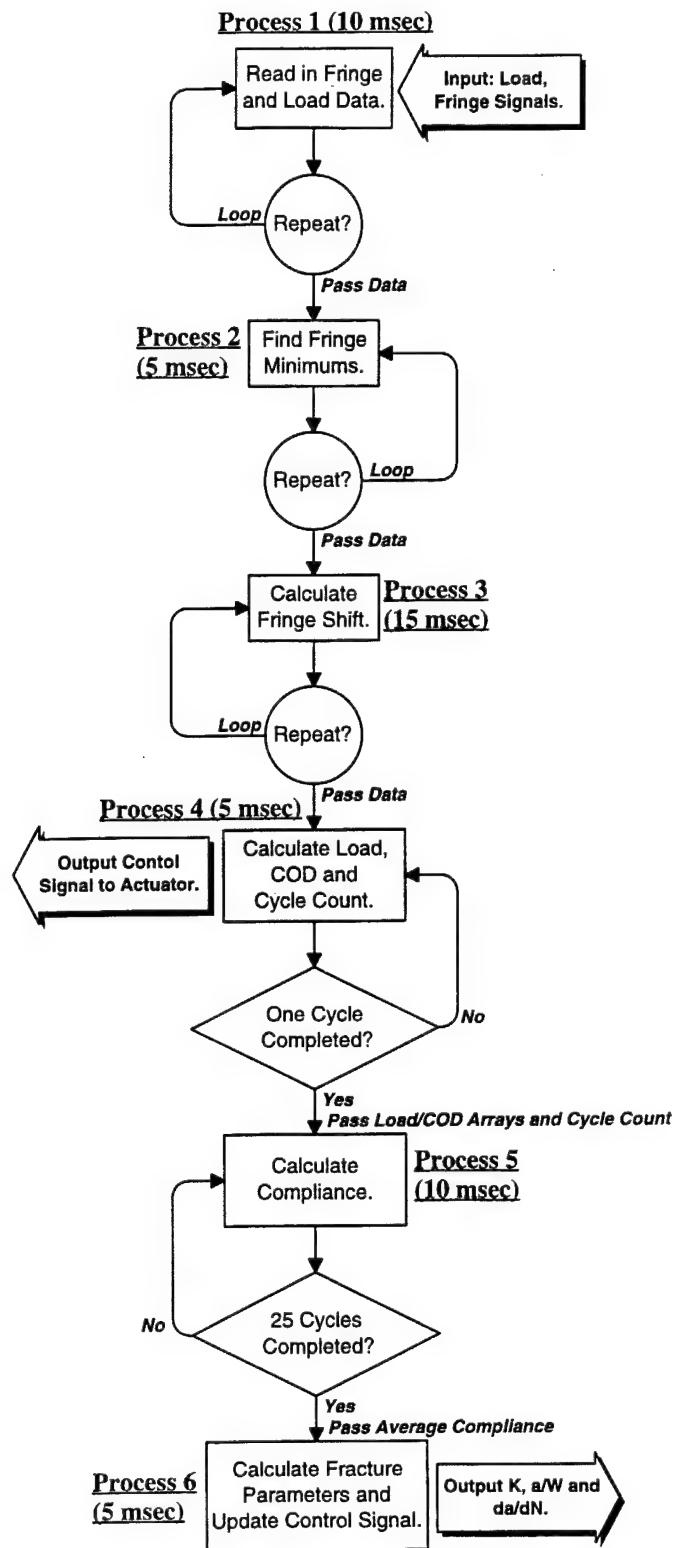


Figure 6
Data Acquisition System Logic

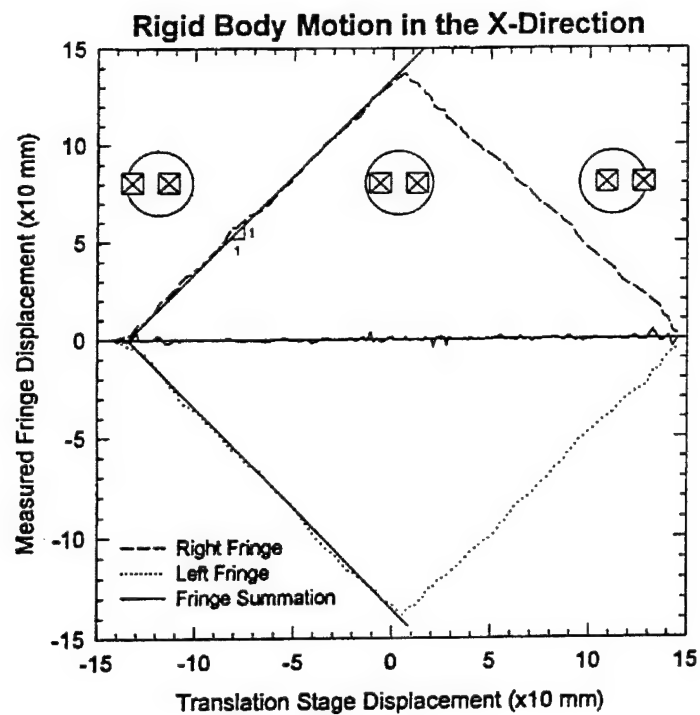


Figure 7
Rigid Body Motion in the X Direction

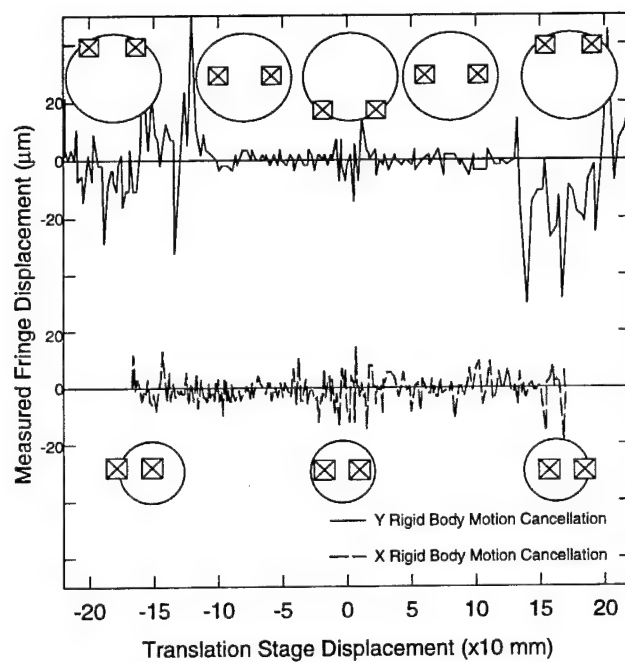


Figure 8
Combined Rigid Body Motion

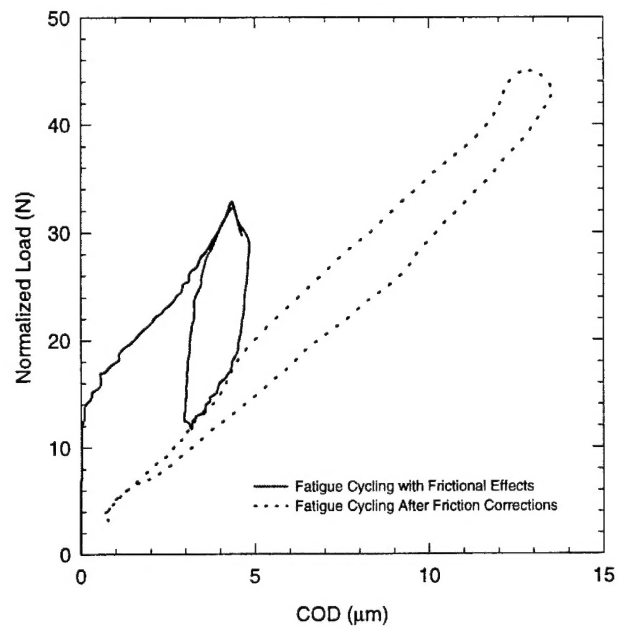


Figure 9
Frictional Effects on Fatigue Cycling

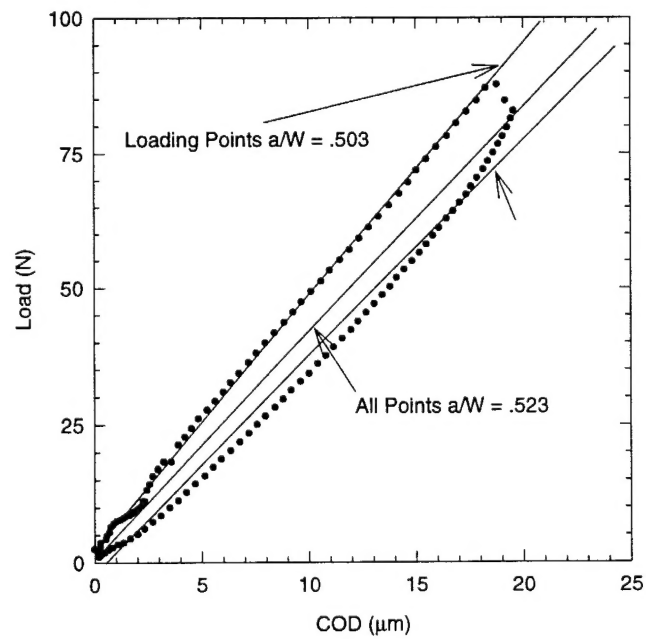


Figure 10
Compliance Estimates During Quasistatic Loading

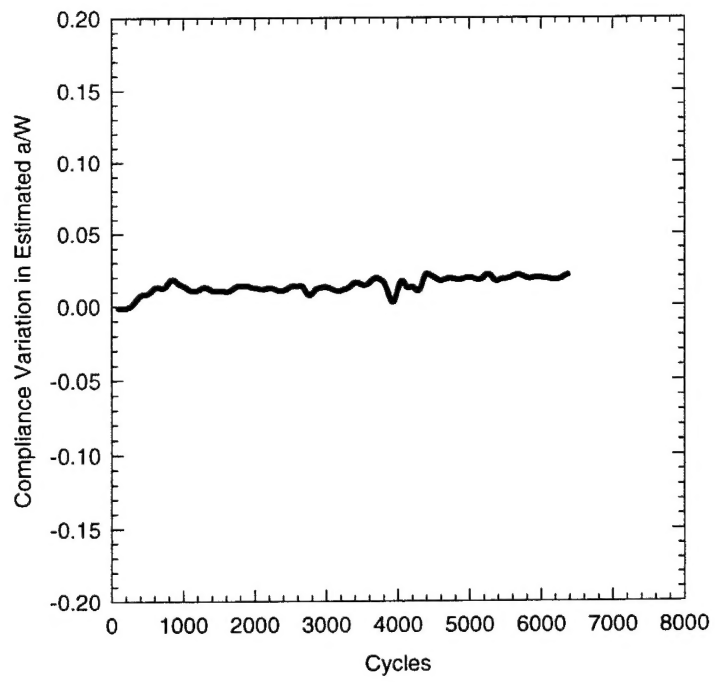


Figure 11
System Stability

REFERENCES

- 1 Amayev, A.D., et al. "Use of Subsize Specimens for Determination of Radiation Embrittlement of Operating Reactor Pressure Vessels", Small Specimen Techniques Applied to Nuclear Reactor Vessel Thermal Annealing and Plant Life Extension, ASTM STP 1204, American Society of Testing and Materials, Philadelphia, pp. 424-439, 1993.
- 2 Manahan, M.P., "Determination of Fracture Behavior of Ferritic Steels using Miniaturized Specimens", *Journal of Nuclear Materials* 166, pp. 321-330, 1989.
- 3 Sharpe, W.N., Jr., et al. "New Test Structures and Techniques for Measurement of Mechanical Properties of MEMS Materials", Proceedings of the Symposium on Microlithography and Metrology in Micromachining II, Austin, TX., pp. 78-91, 1996.
- 4 Roy, S., et al. "In Situ Measurement of Young's Modulus and Residual Stress of Thin Electroless Nickel Films for MEMS Applications", Proceedings of the Symposium of the Materials Research Society, Boston, MA., Vol. 365, pp. 573-578 1994.
- 5 Ruggieri, C. and Dodds, R.H., Jr., "A Transferability Model for Brittle Fracture Including Constraint and Ductile Tearing Effects: A Probabilistic Approach", *Int. Journal of Fracture*, Vol. 79, pp. 309-340, 1996.
- 6 Xia, L. and Shih, C.F., "Ductile Crack Growth -J. A Numerical Study Using Computational Calls with Microstructurally Based Length Scales", *Journal of the Mechanics and Physics of Solids*, Vol. 41, pp. 835-861, 1993.
- 7 Sharpe, W.N., Jr., "An Interferometric Strain/Displacement Measurement System," NASA Technical Memorandum 101638, August 1989.
- 8 Sharpe, W.N., Jr., "Applications of the Interferometric Strain Displacement Gage," Optical Engineering, Vol. 21, No. 3, pp. 483-488, 1982.
- 9 Sharpe, W.N., Jr., "The Interferometric Strain Gage," *Experimental Mechanics*, Vol. 8, No. 4, pp. 164-170, 1968.
- 10 Hartman, G., and T. Nicholas, "An Enhanced Interferometric System for Measuring Crack Displacements," *Experimental Techniques*, Vol. 11, pp. 24-26, 1987.
- 11 Sharpe, W.N., "Crack-Tip Opening Displacement Measurement Techniques," Experimental Techniques in Fracture, VCH Publishers, Inc., New York, NY., pp. 219-251, 1993.
- 12 Young, M., Optics and Lasers, 3rd Ed. New York: Springer, 1886.
- 13 ASTM E 1820-96, "Standard Test Method for Measurement of Fracture Toughness." American Society of Testing and Materials, Philadelphia, PA. 1996.
- 14 O'Dowd, N.P., "Family of Crack-Tip Fields Characterized by a Triaxiality Parameter: Part I - Structure of Fields", *Journal of the Mechanics and Physics of Solids*, Vol. 39, pp. 983-1015, 1991.
- 15 Shih, C.F. and German, M.D., "Requirements for a One Parameter Characterization of Crack Tip Fields by the HRR Singularity", *Int. Journal of Fracture*, Vol. 17, pp. 27-43, 1985.

DISTRIBUTION LIST

<u>Copies</u>	<u>Outside Distribution</u> <u>Agency</u>	<u>Copies</u>	<u>Center Distribution</u> <u>Code</u>
4	NAVSEA	1	0112(Douglas)
1	SEAO3M	1	0115 (Messick)
1	SEA 03M2 (Null)	1	60 (Wacker)
1	SEA 03P (McCarthy)	1	601 (Morton)
1	SEA 03P2 (Nichols)	1	601 (Barkyoumb)
		1	602 (Rockwell)
2	DTIC	1	603 (Cavallaro)
		1	604 (Desavage)
3	ONR	1	605 (Fisch)
1	1131 (Yoder)	1	606
1	1131 (Sedricks)	1	61 (Holsberg)
1	332 (Vasudevan)	1	61s
		1	62 (Eichenger)
4	NRL	1	63 (Alig)
1	Code 6310	1	64 (Fischer)
1	Code 6312 (Bayles)	1	65 (Beach)
1	Code 6314	1	66 (Riley)
1	Code 6316	1	67 (Hansen)
		1	68 (Mueller)
2	NRC	1	611 (Palko)
1	EMMB/DET/RES (Vassilaros)	1	612 (Aprigliano)
1	EMMEB/DET/RES (Malik)	3	613 (Ferrara)
		1	614 (Monternarano)
		10	614 (Czyryca)
		10	614 (Tregoning)
		15	614 (Mercier)
		1	614
		1	615 (Denale)
		1	3421
		1	3422
		1	3431